

## ON THE 3D DYNAMICS OF THE WAKE BEHIND A CIRCULAR CYLINDER

V. Uruba<sup>1,2</sup>, P. Procházka<sup>1</sup>, V. Skála<sup>1</sup>

<sup>1</sup> Department of Fluid Dynamics, Institute of Thermomechanics of the Czech Academy of Sciences, Dolejškova 5, 182 00, Czech Republic

<sup>2</sup> Department of Power System Engineering, Faculty of Mechanical Engineering, University of West Bohemia, Universitní 8, 306 14 Plzeň, Czech Republic

### Abstract

Flow in the wake of a circular cylinder is studied experimentally using time-resolved stereo PIV method. Special attention is paid to 3D topology of dynamical structures. While the distribution of statistic quantities along the cylinder is uniform, and i.e. 2D, the instantaneous flow structure is fully 3D. Within the velocity fluctuating flow field the structures containing streamwise vorticity and velocity components are dominant. The POD modes connected with von Kármán vortex street are identified.

**Keywords:** circular cylinder, wake, 3D structure, POD

## 1 Introduction

Many kinds of flows in practical applications could be characterized by 2D boundary conditions. Typical example could be the case of cross-flow around a prismatic body. In spite of inherent dynamical nature of the turbulent flow-field, this case could be considered as a plane flow, invariant along the body (excluding the ends). Such a case is also mathematically modelled as a 2D flow very often, taking into account only a single cross-section, supposing the same flow picture for any other cross-section along the body.

The case of circular cylinder in cross-flow belongs to so called canonical cases. We could find extensive information on this case in literature, theoretical, experimental and numerical studies. Most of available studies treat the prismatic cylinder as forced 2D case, no 3D structures are detected see e.g. [1]. The 3D structure of the wake behind a body of 2D geometry has been already addressed e.g. in [2]. The paper [3] deals with the d'Alembert paradox (zero forces) for inviscid flow and shows that this paradox is due to forced 2D stationary flow pattern, which is however instable under a specific conditions. In the real 3D nonstationary flow the forces are generated even in the inviscid case and the d'Alembert paradox is thus resolved.

The wake behind a circular cylinder is to be studied experimentally using PIV. Dynamics of the wake will be analysed with help of the POD method, special attention is paid to the 3D effects. Changes of the flow-field in spanwise direction are to be studied in detail. Special attention will be paid to streamwise velocity and vorticity components dynamical topology.

It is known that the wake behind circular cylinder exhibits several types of flow patterns: steady, unsteady periodical and chaotic, the universal control parameter is the Reynolds number based on cylinder diameter  $d$ , incoming flow velocity  $U_{in}$  and fluid kinematic viscosity  $\nu$ :

$$Re = \frac{U_{in} d}{\nu}. \quad (1)$$

Description of the wake topology including its dynamics could be found in any good book on fluid mechanics, where more information could be found, see e.g. [1].

## 2 Experimental Setup

The experimental setup is to be introduced now. The blow-down facility in IT ASCR with closed test section  $250 \times 250 \text{ mm}^2$  has been used. The cylinder model of diameter  $d = 15 \text{ mm}$  across the test section, from wall to wall. It is placed perpendicularly to the flow, the flow-field was with low turbulence (about 0,2 %) and good regularity (departures below 1 %), mean velocity  $U_{in} = 5 \text{ m/s}$  resulting in Reynolds number 4 815. Effect of higher Reynolds numbers values has been shown in [4].

## 2.1 Boundary Conditions

The measuring planes are shown in Fig. 1, the streamwise oriented Plane of Measurement (PoM) number 1 ( $xy$ ) in green, while the cross-oriented PoM 2 ( $yz$ ) is shown in red. The PoM 2 is in distance  $3.83 d$  from the cylinder axis in the streamwise direction.

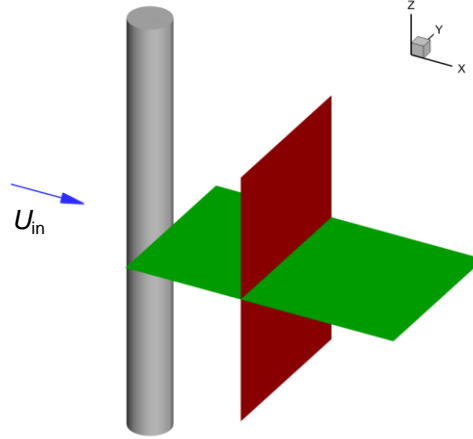


Figure 1: Schematic view on the experiment.

The Cartesian coordinate system is defined with  $x$ -axis in streamwise direction and  $z$ -axis forming the cylinder axis of rotation.

## 2.2 Methods of Measurement

The velocity vector field was measured using Particle Image Velocimetry (PIV) method. The measurement apparatus consists of laser and CMOS cameras by Dantec company. The laser is New Wave Pegasus, Nd:YLF double head with wavelength of 527 nm, maximal frequency 10 kHz, single shot energy is 10 mJ (for 1 kHz) and corresponding power is 10 W per one head. The cameras Phantom V611 and SpeedSense VEO 410 with resolution of 1 280 x 800 pixels are able to acquire double-snaps with frequency up to 3 kHz (full resolution) and they use internal memory 8 and 18 GB. The data were acquired and post-processed in Dynamic Studio and Techplot software.

For the experiment the time-resolved PIV technique has been applied, acquisition frequency of 2 kHz and time period was 2 s. In the PoM 1, the classical version using a single camera Phantom was applied, evaluating two velocity components  $u$  and  $v$  within the plane of measurement. However, in the PoM 2 the stereo PIV version using two cameras VEO with all necessary accessories was applied. In this case all 3 velocity components  $u$ ,  $v$  and  $w$  were evaluated in the plane of measurement.

The PIV system is described in detail e.g. in [5].

## 2.3 Methods of Data Analysis

Instantaneous velocity fields are analysed using classical statistical methods, mean values and statistical moments: variances and correlations are evaluated.

The flow dynamics was studied using the Proper Orthogonal Decomposition (POD) method, which decomposes the time series of any scalar quantity fields into modes explaining maximum variance in optimal way, starting from the low-order modes. Each POD mode consists of its energy, topology (Topos) and time evolution (Chronos). The details of the POD method are given e.g. in [6,7].

## 3 Results

All results are shown in dimensionless form. The presented velocities are related to the input velocity  $U_{in}$  and the lengths are related to the cylinder diameter  $d$ . Velocities were evaluated in the mesh  $66(x) \times 41(y)$  points in the PoM 1 and  $61(y) \times 91(z)$  in the PoM 2, quantities are interpolated between the points.

The frequencies are given also in dimensionless for of Strouhal number:

$$Sh = \frac{f d}{U_{in}}, \quad (2)$$

where  $f$  is the frequency.

### 3.1 Time Mean Fields

Overview of the time-mean wake structure in the PoM 1 is shown in Fig. 2, where the mean velocity and turbulent kinetic energy fields are depicted. In the vector velocity field the vector-lines are added arbitrarily for better clarity. The position of the PoM 2 is represented by the dashed red line at position  $x = 3,83 d$ .

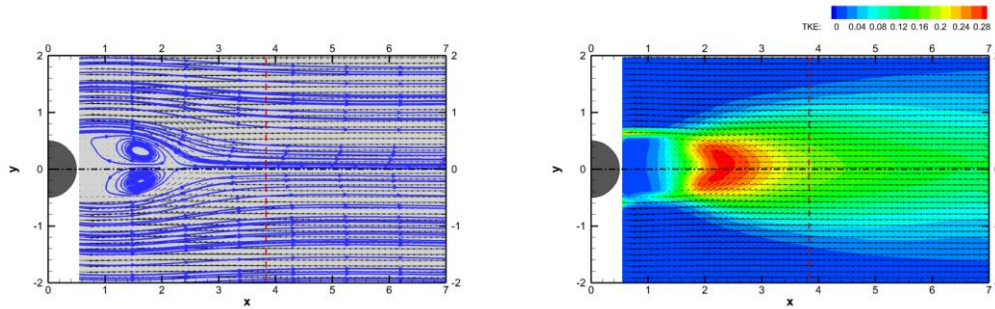


Figure 2: Mean velocity and TKE distributions in the PoM 1.

In Fig. 2 only statistical topology of the wake structure is depicted, the Kármán vortex street is a dynamical structure ([8]) and it is not distinct here. Note, that the distributions in Fig. 2 are symmetrical with the axis of symmetry  $x$  ( $y = 0$ ).

The distribution of the time-mean streamwise velocity component  $U$  in the transversal PoM 2 is shown in Fig. 3. Projection of the cylinder silhouette in  $x$  streamwise direction is demonstrated by dashed lines, the dash-dot line represents the cylinder axis.

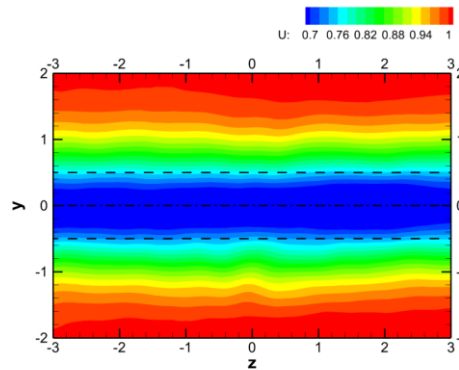


Figure 3:  $U$  velocity component distribution in the PoM 2.

The distribution of  $U$  along the  $z$  axis is close to be homogeneous, the  $U$  values are not dependent on  $z$  position. The same could be said about the other time-mean characteristics including variations of velocities and statistics related to velocity and vorticity. Thus, those quantities are averaged along the  $z$  lines resulting in  $y$  graphs.

In Fig. 4 graphs of  $U$  and  $U_{std}$  (standard deviation) as well as Turbulent Kinetic Energy (TKE)  $z$ -averaged as functions of position  $y$  are shown. Position of the cylinder projection is shown here as well.

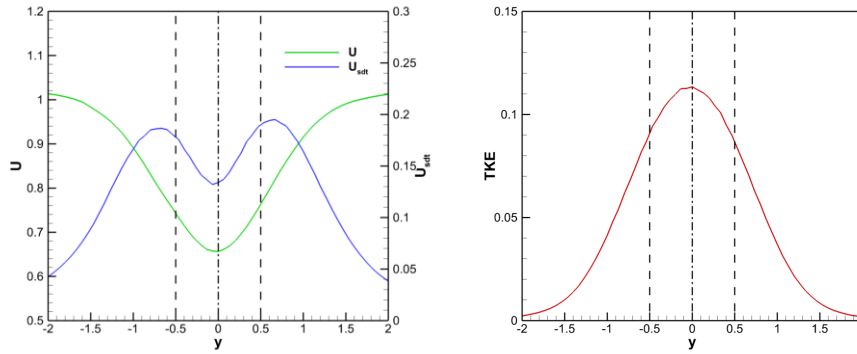


Figure 4: Streamwise velocity, its standard deviation and TKE.

The mean velocity has its minimum on the cylinder axis, which is the wake centre-axis in the same time. The streamwise velocity component standard deviation has two maxima close to the cylinder contour. However the Turbulent Kinetic Energy shows a single maximum in the centre.

The correlation coefficients of the velocity components are evaluated for all 3 possible combinations and shown in Fig. 5 left-hand part. This quantity could be linked to Reynolds stress components and in the end to the turbulence production process. While the  $r_{uw}$  and  $r_{vw}$  are relatively small in absolute value, the  $r_{uv}$  has its extremes in positions  $y = \pm 1$  and it is anti-symmetrically distributed. The two locations indicate maxima of turbulence production.

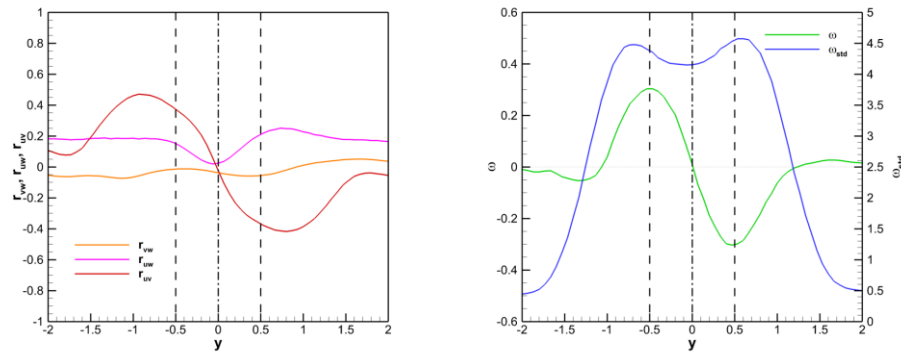


Figure 5: Correlation coefficients and vorticity.

On the right-hand part of the Fig. 5 the streamwise vorticity  $\omega_x$  and its standard deviation distributions are shown. Extremal values of both mean vorticity value and its standard deviation are located again close to the cylinder silhouette. Please note, that the mean vorticity extremes are of opposite signs and the standard deviation value is order of magnitude higher than the mean value.

In general, all statistical quantities are symmetrically or anti-symmetrically distributed along the  $y$  axis.

### 3.2 Cross-Plane Dynamics

First the POD procedure is to be applied on the PoM 1 result. In Fig. 6 there are two dominant POD modes Topos 1 and 2 covering 35 and 33 % of the total kinetic energy corresponding to the streamwise velocity component respectively. The relative Chronoses representing time evolution of the modes exhibit strong peak on the frequency  $f_1 = 70$  Hz. This frequency is the dominant frequency characterizing the von Kármán vortex street process. The corresponding Strouhal number  $Sh$  is here about 0.2, this value is in accordance with theses referred in the literature (e.g. [9]).

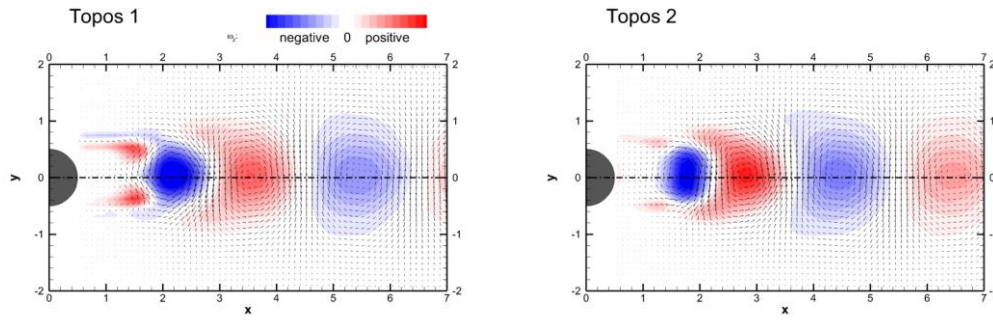


Figure 6: The dominant POD modes in PoM 1.

The colour represents vorticity evaluated from in-plane velocity components. The POD modes 1 and 2 represent two phases of vortex street structure represented by a wave of vortices of alternative orientation: positive (red) and negative (blue). The modes are shifted by phase angle  $\pi/2$ .

### 3.3 Streamwise Velocity Dynamics

Now, the data acquired using stereo PIV technique within the PoM 2 is subjected to POD analysis. Only the streamwise velocity component  $U$  is taken into account.

In Fig. 7 the energy budget of the  $U$  POD analysis is shown,  $E$  is kinetic energy fraction of the given  $U$  POD mode,  $E_a$  is accumulated kinetic energy fraction, i.e. sum all lower modes energy fractions and  $E_r$  is residual kinetic energy fraction, i.e. the energy fraction not covered by the  $E_a$ . Please note that the kinetic energies reflect only streamwise velocity component.

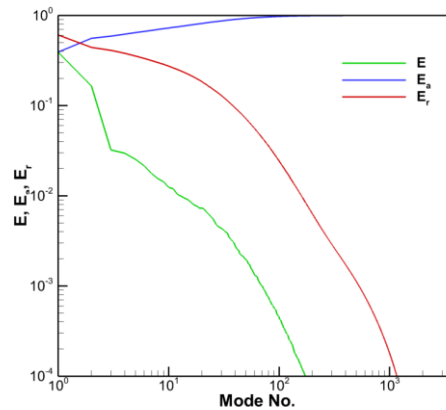
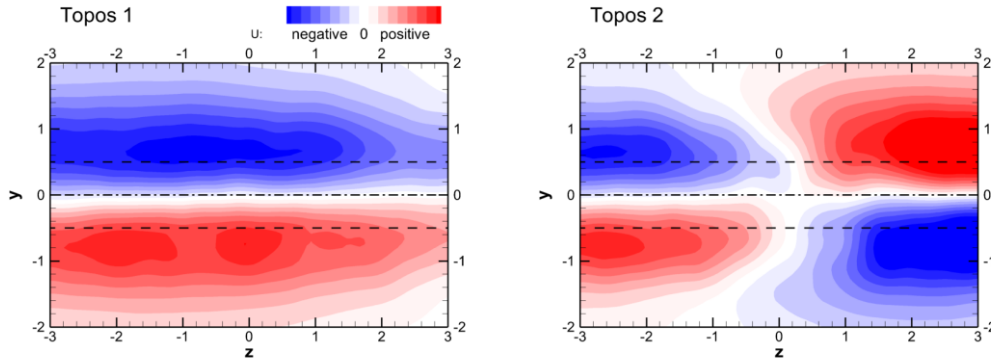


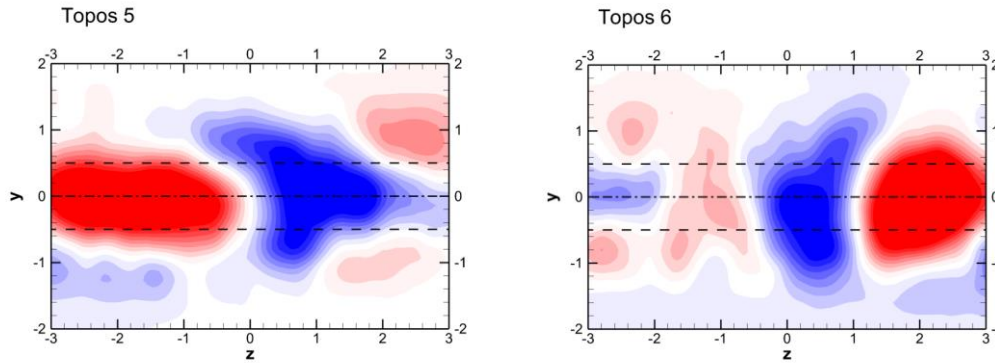
Figure 7: Energy budget of  $U$  velocity component POD analysis

The  $U$  POD modes are categorized according to their frequency content into several groups. The basic frequency  $f_1$  is the Strouhal frequency corresponding to the von Kármán vortex street. Its value is 70 Hz and corresponding Strouhal number 0,2. In the Chronos content also the higher frequencies are present  $f_2 = 2f_1$  (= 140 Hz) and  $f_3 = 3f_1$  (= 210 Hz), moreover, very low frequency  $f_0 = 10$  Hz could be detected in some Chronoses. Generally, the modes containing peaks on the Strouhal frequency  $f_1$  and/or its harmonics  $f_2, f_3$  are very probably linked with von Kármán vortex street phenomenon. Another type of Chronos frequency spectrum is fully dense spectrum over a given range of frequencies, without any distinct peaks. The first group of  $U$  POD modes is characterized by the single frequency  $f_1$  in spectrum. The  $U$  POD mode 1 covers about 40 % of total kinetic energy, while the mode 2 covers 20 % of it. The Topos 1 represents  $U$  pulsations in opposite phase in the upper and lower parts of the PoM. Please note that the mode 1 is close to 2D geometry. Maximal amplitudes of those pulsations are located close to the cylinder silhouette.

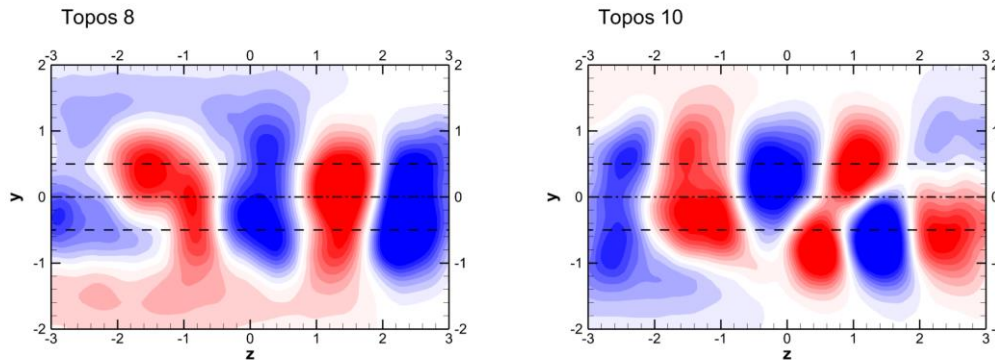
The Topos 2 topology is divided into 4 regions with alternative pulsations. The Toposes 1 and 2, which are typical representatives of the first group, are shown in Fig. 8.

Figure 8: Topos  $U$  modes 1 and 2,  $f_1$ .

The next group of the  $U$  POD modes is characterized by 3 distinct peaks in the Chronos spectrum on the 3 harmonics  $f_1$ ,  $f_2$  and  $f_3$ . The amplitudes of the peaks are decaying for the higher harmonics. The  $U$  POD modes 5 and 6 cover 1.7 and 1.3 % of total kinetic energy respectively. The pulsations are concentrated close to the cylinder axis.

Figure 9: Topos  $U$  modes 5 and 6,  $f_1$ ,  $f_2$  and  $f_3$ .

The next type of  $U$  POD modes is characterized by the frequencies  $f_0$  and  $f_2$  only, i.e. combination of a very low frequency and the second harmonics. As an example the  $U$  POD modes 8 and 10 are shown in Fig. 10, they cover 1.1 and 0.9 % of total kinetic energy respectively.

Figure 10: Topos  $U$  modes 8 and 10,  $f_0$  and  $f_2$ .

Topology of the modes is characterized by spots of positive and negative pulsations within the wake. The spots are smaller for higher mode order.

This is true also for the next  $U$  POD modes group characterised by dense frequency spectrum without any distinct frequency peaks. This character is typical for the modes of order 12 and higher. As an example the modes 12 and 30 are shown in Fig. 11. Those modes cover 0.7 and 0.3 % of total kinetic energy respectively.

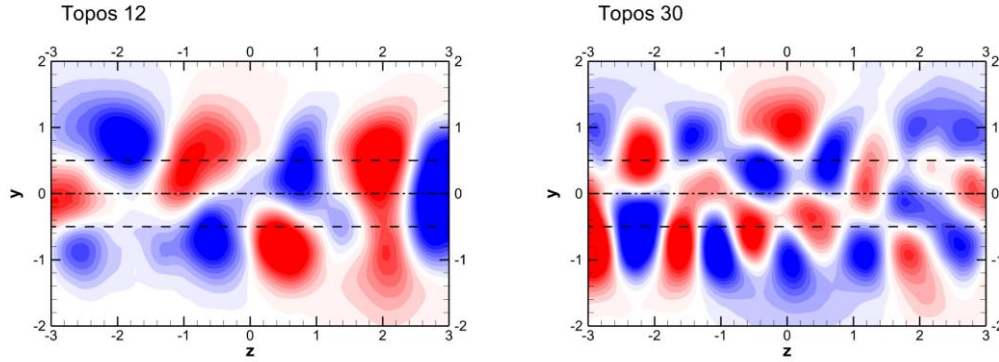


Figure 11: Topos  $U$  modes 12 and 30, dense spectrum.

The low-order  $U$  POD modes with high energy could be linked with the von Kármán vortex street generation process. The higher order modes are characterised by dense spectrum and could be linked with the turbulent structure of the wake.

### 3.3 Streamwise Vorticity Dynamics

The streamwise vorticity component  $\omega_x$  distribution was evaluated from the velocity snapshots. The mean value and standard deviation distributions are homogeneous in  $z$  direction, evolution in  $y$  direction is shown in Fig. 5 above. The POD procedure was applied on the vorticity data. The primary raw data used for this analysis is identical with the source data for the streamwise velocity dynamics analysis shown above.

In general, if the POD analysis is applied on a vorticity data, the enstrophy  $S$  becomes the relevant quantity. In Fig. 7 the enstrophy budget of the  $\omega_x$  POD analysis is shown, meaning of the subscripts (“a” and “r”) is the same as for the kinetic energy in the velocity POD case, see above. So,  $S$  stands for the enstrophy fraction,  $S_a$  is accumulated enstrophy fraction, i.e. sum all lower modes enstrophy fractions and  $S_r$  is residual kinetic energy fraction, i.e. the enstrophy fraction not covered by the  $S_a$ . All enstrophies are related merely to the streamwise vorticity component.

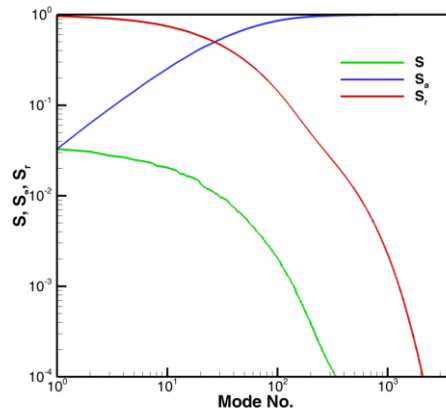


Figure 12: Enstrophy budget of  $\omega_x$  velocity component POD analysis

The total enstrophy is distributed much more regularly across the  $\omega_x$  POD modes than the kinetic energy for the  $U$  POD, compare with Fig. 7.

Unlike the  $U$  POD mode, the  $\omega_x$  POD modes could be categorized into two only. The modes 1, 2 and 3 contain the frequency peaks on  $f_1$  and  $f_3$  in the Chronos spectrum, the second harmonics is not present. Those modes could be linked to the von Kármán vortex street process. The higher order  $\omega_x$  POD modes are characterised by dense Chronos spectrum and thus they could be linked with the wake turbulence.

As an example of the first  $\omega_x$  POD modes category, the modes 1 and 2 are to be shown in Fig. 13, which cover 3.3 and 3.1 % of total enstrophy respectively.

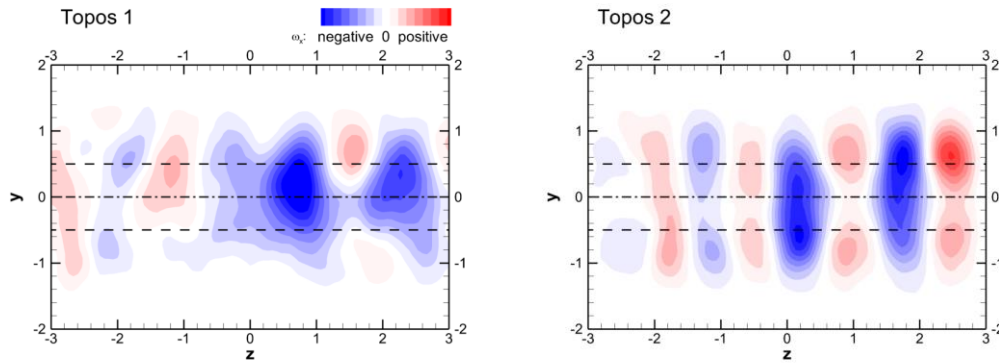


Figure 13: Topos  $\omega_x$  modes 5 and 6,  $f_1$ , and  $f_3$ .

The spots of streamwise vorticity are distributed along the  $z$  axis within the wake. The vortices are elliptical and they cover virtually the whole width of the cylinder wake.

The higher order modes with dense spectrum represent turbulent behaviour within the wake. In Fig. 14, the  $\omega_x$  POD modes 12 and 30 are shown. The wake is filled by small vortices in more or less homogeneous manner. The higher mode order, the smaller vortices and better homogeneity could be detected.

The  $\omega_x$  POD modes 12 and 30 cover 1.9 and 0.9 % of total enstrophy respectively.

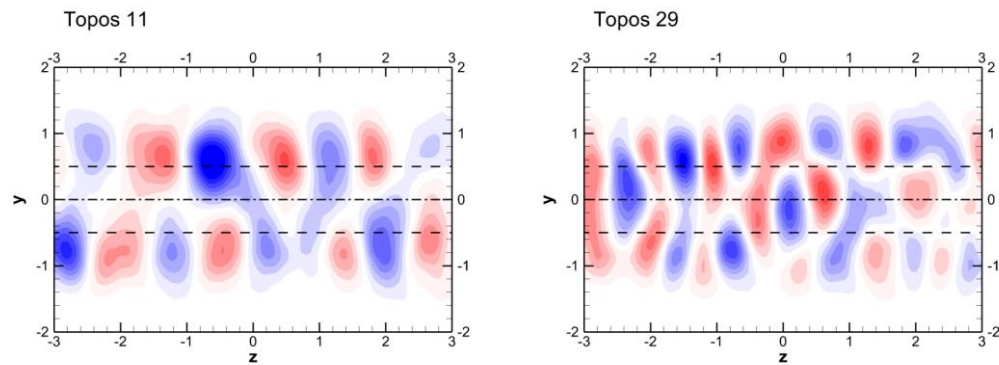


Figure 14: Topos  $\omega_x$  modes 12 and 30, dense spectrum.

The  $\omega_x$  POD results indicate highly random distribution of the fluctuating streamwise vorticity along the cylinder and weak link to the von Kármán vortex street process.

## 4 Conclusions

The POD analysis of the streamwise velocity and vorticity components  $U$  and  $\omega_x$  is presented in the paper. The POD modes linked with the von Karman vortex street process are identified and they are

characterized by the Strouhal frequency and higher harmonics. The flow dynamics connected with this phenomenon is highly 3D and contains pulsation of both streamwise velocity component and vorticity. The streamwise vorticity seems to be an important attribute of the cylinder wake dynamics; however it is linked with the von Karman vortex street process only weakly. The fundamental role in the cylinder wake dynamics plays the velocity fluctuations.

The topological structures distributed along the cylinder axis are not present in the mean flow-field, which is close to the 2D structure, independent on  $z$  position along the cylinder axis.

Recently, the streamwise vorticity dynamics has been identified in the wake behind inclined plate, compare with [10].

## Acknowledgement

This work was supported by the Grant Agency of the Czech Republic, projects Nos. 17-01088S, 19-04695S and 19-02288J.

## References

- [1] White, F.M.: Fluid Mechanics. *McGraw Hill*, (2015).
- [2] Uruba V.: On 3D instability of wake behind a cylinder, *AIP Conference Proceedings*, vol. 1745, (2016) art. no. 020062
- [3] Hoffman J., Johnson C.: Resolution of d'Alembert's paradox, *J. Math. Fluid Mech.*, vol. 12, no. 3: (2010) pp.321-334
- [4] Uruba, V., Procházka, P.: The Reynolds number effect on dynamics of the wake behind a circular cylinder. *AIP Conference Proceedings*, vol. 2189: (2019) art. no. 020023
- [5] Procházka P., Uruba V.: Streamwise and spanwise vortical structure merging inside the wake of an inclined flat plate, *Mechanics&Industry*, vol. 20, issue 7: (2019) 705, 13 pp.
- [6] Uruba V.: Decomposition methods in turbulent research, *EPJ Web of Conferences*, vol. 25: (2012) 01095
- [7] Uruba, V.: Energy and Entropy in Turbulence Decompositions, *ENTROPY*, vol. 21, issue 2: (2019) art. no. 124, 18 pp.
- [8] Williamson, C.H.K.: Vortex Dynamics in the Cylinder Wake, *Annu. Rev. Fluid. Mech.*, vol. 28: (1996) pp. 477-539
- [9] Roshko A.: On the development of turbulent wakes from vortex streets. NACA Rep. 1191: (1955) pp.801-825
- [10] Uruba V., Pavlík D., Procházka P., Skála V., Kopecký V.: On 3D flow-structures behind an inclined plate, *EPJ Web of Conferences*, vol. 143: (2017) art. no. 02137